DOI: 10.31276/VJSTE.63(2).25-31

A simple approach for air-gap permeance calculations in double excitation synchronous motor modelling with reluctance network

Trung-Kien Hoang[1*], L. Vido[2], Dinh-Quang Nguyen[3]

[1]*Graduate University of Science and Technology, Vietnam Academy of Science and Technology, Vietnam*
[2]*SATIE, Cergy - Pointoise University, France*
[3]*Institute of Energy Science, Vietnam Academy of Science and Technology, Vietnam*

Received 3 July 2020; accepted 28 October 2020

Abstract:

This article proposes an easy-to-use approximation for air-gap permeance calculations in a reluctance network. An extension of the overlap area between the stator and its corresponding rotor tooth to a position where the permeance becomes zero is also proposed. The advantage of this method is the simplification of conventional complex reluctance calculations while maintaining high accuracy. The proposed approach is applied to a double excitation synchronous motor, which usually requires a 3D simulation tool for the calculations. The validation of the accuracy of the proposed method on the flux linkage, back EMF, and electromagnetic torque are accomplished by comparison with those obtained from a conventional method and experimental data. The results of the comparison recommend the use of the proposed method for different electrical motor geometries.

Keywords: **double excitation, reluctance network, 3D simulation.**

Classification number: **2.3**

Introduction

A double excitation synchronous motor (DESM) combines permanent magnets and excitation windings to form the double excitation principle. The advantages of permanent magnets and windings is that they satisfy the requirements of railway traction applications that require a wide range of motor operations. Several papers have been published that focus on DESM [1-4].

The finite element method (FEM) is a traditional tool that is capable of highly accurate results. However, FEM is time consuming and, further, 3D FEM makes the optimisation design stage of a motor impossible. As an alternative, the reluctance network (RN) method provides fast, ready-to-analyse results while good accuracy is still maintained. This method transforms the motor into a magnetic circuit represented by nodes, reluctances, and magneto-motive forces (MMF). The RN method is widely employed in electric motor analysis [5-8].

One of the key components of the RN model is the air-gap permeance, which varies according to the relative position between the rotor and stator [9]. In order to calculate air-gap permeance, flux paths through the air-gap are often structurally approximated [10-13]. In the simplest approach, the air-gap flux is bounded by an overlapped area between the stator and rotor teeth. In [10], a permeance evolution law is defined to connect a stator tooth to a rotor tooth. In [11], the Schwarz-Christoffel transformation was used to calculate the air-gap permeance for a simple 2D air-gap configuration such as that of transformer cores. In [12], the air-gap permeance is well approximated considering every possible flux path between the stator and rotor teeth. In this paper, the authors propose to calculate the air-gap permeance by extending the overlapped area between the stator and its corresponding rotor tooth to the position where the permeance becomes zero. To examine the validity of the proposed approach, the results are compared with the ones obtained by the method in [12] and experimental measurements.

*Corresponding author: Email: hoang-trung.kien@usth.edu.vn

Reluctance network method with DESM

DESM model configuration

The studied model of the DESM is displayed in Fig. 1 [3].

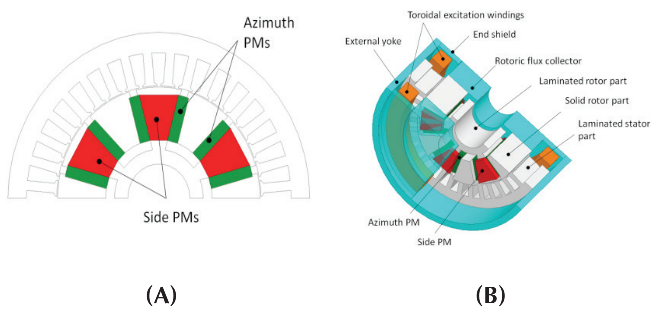

Fig. 1. The DESM model (A) the arrangement of permanent magnets (PMs) in a 2D and (B) a 3D view.

In the configuration of Fig. 1 (phase windings are not shown for clarity), two toroidal excitation windings are placed in the stator. Ferrite permanent magnets (PMs) are placed in the rotor to increase the air-gap flux density under the flux focusing principle. The stator has a conventional laminated core while both solid and laminated cores are used in the rotor due to the presence of 3D flux paths.

RN method

In this article, the flux tube method is employed. This is the most popular implementation of the RN method, which was proposed by V. Ostovic [10]. Each part of the machine is represented by the reluctance limited by a flux tube. Inside the tube, the flux is assumed to be constant. A basic expression for the reluctance of the flux tube can be given by Eq. 1 [2]:

$$R = \frac{l}{\mu_r \mu_0 S} \tag{1}$$

where l is the length, S is the cross section of the flux tube, μ_r is the relative permeability of the tube's material, and μ_0 is the absolute permeability of the air. For the air and PMs, μ_r equals unity and for the core, μ_r is computed based on the nonlinear magnetization curve of the core material.

A permanent magnet can be modelled by a reluctance connected in series with an equivalent MMF as in Eq. 2:

$$M_{PM} = \frac{B_r}{\mu_r \mu_0} h_m \tag{2}$$

where h_m and B_r are the magnet thickness and remanence, respectively.

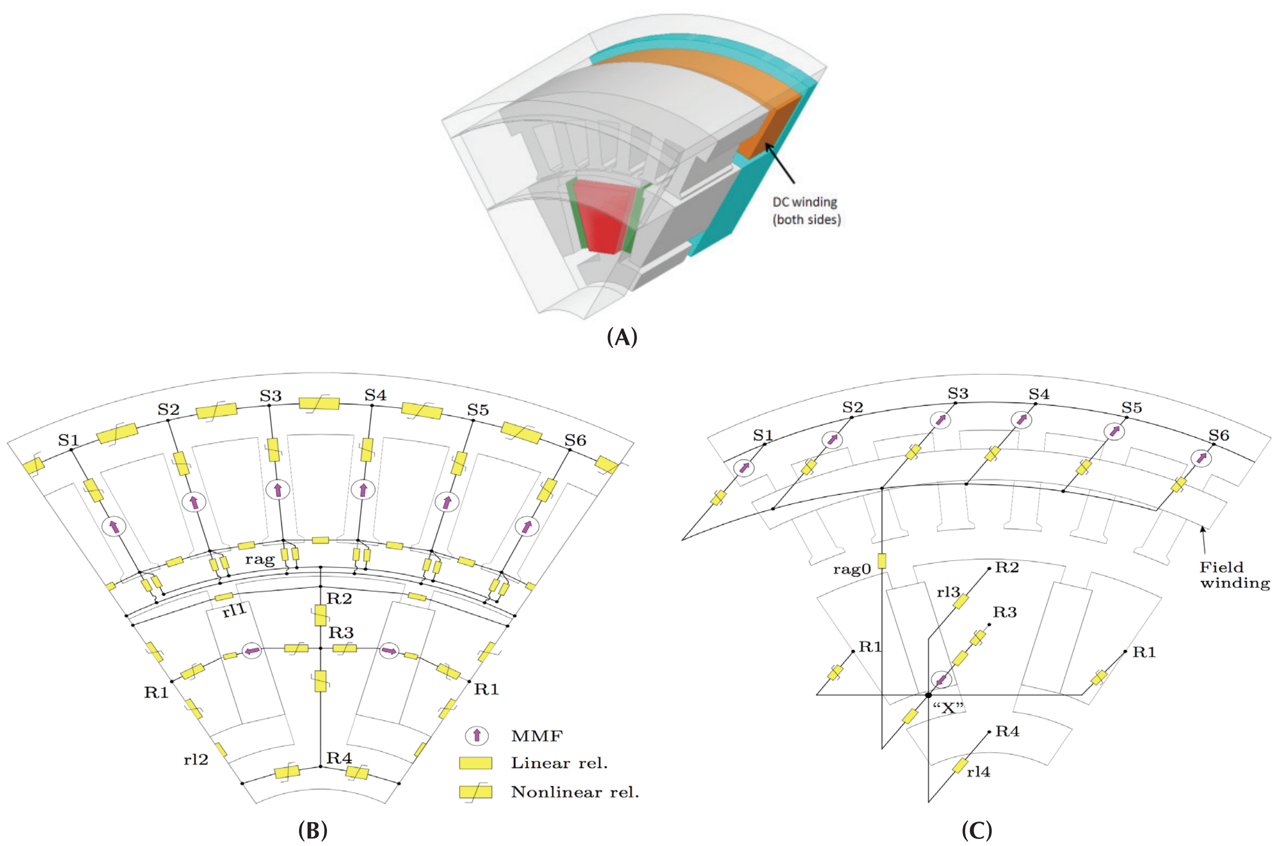

Fig. 2. The RN model of the studied DESM (A) one pole pair for modelling, (B) first part of the RN, and (C) second part of the RN (in the axial direction).

Figure 2 presents the reluctance model, which is defined for one pole pair. The air-gap length is exaggerated to be large for ease of observation.

The reluctance model is comprised of two parts. The first part, presented in Fig. 2B, consists of the stator, rotor, phase windings, and azimuth magnets. The second part, with one of its two identical sides shown in Fig. 2C, is composed of the external yoke, rotoric flux collectors, excitation windings, side magnets, and end shields. The purpose of the second part is to conduct the flux along the third dimension. This flux begins at the stator, goes through the air-gap reluctance (Fig. 2B) and then passes through the side PMs, rotoric collector, outer air- gap reluctance (Fig. 2C), and the end shield before returning to the stator. In Fig. 2B, the phase MMFs are put in the stator teeth and the net MMF is given by Eq. 3:

$$M_{phase} = (I_1 - I_2)N_c \tag{3}$$

where N_c is the number of turns in the phase winding, and I_1 and I_2 are the phase currents flowing through the winding placed in the slot.

In this model, two reluctances are used to connect a stator tooth to two rotor poles. The flux is assumed to be perpendicular to the stator and rotor tooth surfaces. In this sense, the tangential component of the air-gap flux density is neglected. In the simplest manner, the air-gap flux path is confined to the overlapped area between the rotor pole and stator tooth. Improved approximations to mitigate the fringing effect will be discussed in next section.

Air-gap permeance calculations

Air-gap permeance with detailed flux fringing path

In comparison to the permeances of the ferromagnetic regions and permanent magnets, the permeances of the air-gap region are more complicated because of their flux fringing paths as displayed in Fig. 3. To simplify the complex flux paths, the authors in [12] assume an equipotential on the stator and rotor surface flux paths that are perpendicular to the tooth surfaces.

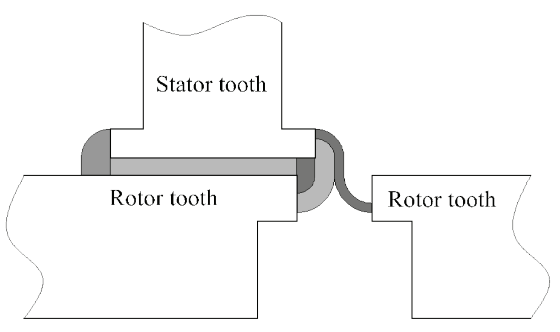

Fig. 3. Fringing effect illustration in the air-gap region.

Figure 4 shows several typical flux paths and permeance calculations in the air-gap. Given a motor geometry, all possible flux paths can be approximated according to the above assumptions.

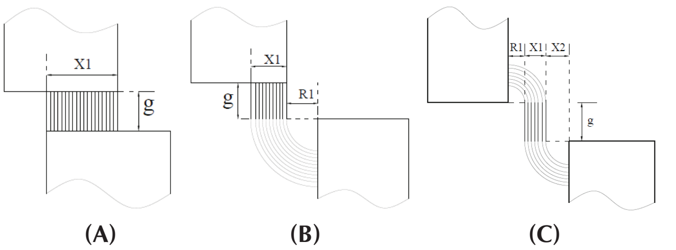

Fig. 4. Typical air-gap permeance.

The permeance for the air-gap in Figs. 4A, 4B, and 4C can be calculated from Eqs. 4-6, respectively [12]:

$$P = \frac{\mu_0 L_a X_1}{g} \tag{4}$$

$$P = \frac{2\mu_0 L_a}{\pi} \ln\left(1 + \frac{\pi X_1}{\pi X_1 + 2g}\right) \tag{5}$$

$$P = \frac{\mu_0 L_a}{\pi} \ln\left(1 + \frac{2\pi X_1}{\pi(R_1 + R_2 + 2g)}\right) \tag{6}$$

where L_a is axial length of the teeth, other variables are shown in Fig. 4.

This approach considers every flux fringing path in detail; however, the difficulty is that every combination of relative positions between the stator and rotor teeth must be considered. For example, the prototype of the DESM in the present work has 17 relative positions to be analysed and each position includes several functions to determine the permeances of different flux paths. The air-gap permeance between the stator and rotor teeth as function of the stator tooth position is shown in Fig. 5.

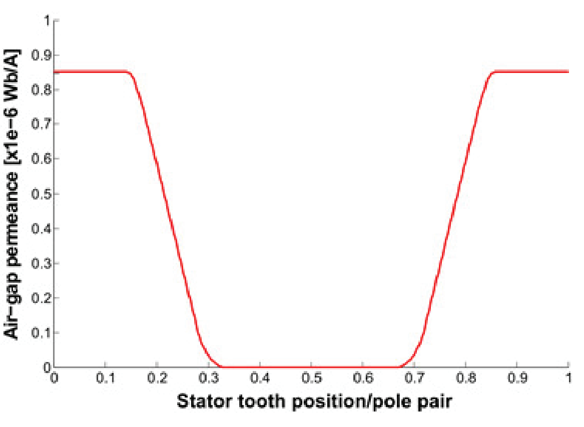

Fig. 5. Air-gap permeance as function of the stator tooth position.

Simple approximation method

In response to the time-consuming nature of considering every possible flux path presented in the air-gap permeance approximation above, this paper proposes an approach to further simplify the calculations. The overall strategy is to define a new approach that simplifies the process while keeping the air-gap permeance closely matched to the one obtained by the traditional approach. The permeance curve shown in Fig. 5 consists of three different types: the maximum permeance, zero permeance, and the transition between those two values. The approach proposed in this article determines the positions in which the air-gap permeances are maximum and minimum (zero). A linear transition from maximum to zero is proposed. This is based on the fact that the transition displayed in Fig. 5 is mostly linear.

The air-gap permeance is a maximum value when the overlapped area is maximized as shown in Fig. 6. The approach in [12] presents three different flux paths, however, in this work, these three flux paths are replaced by one equivalent path. The overlapped area will, therefore, be extended to create the same permeance as calculated in [12]. In the proposed method, the overlapped area will be extended by 0.41 mm to each side of the stator tooth, which is approximately equivalent to 80% of the air-gap length (g=0.5 mm). In a general case, the extended area is suggested to be between 0.8 to 1.0 times the air-gap length. The air-gap permeance remains constant until the right edge of stator tooth reaches the right side of rotor tooth as illustrated in Fig. 6C.

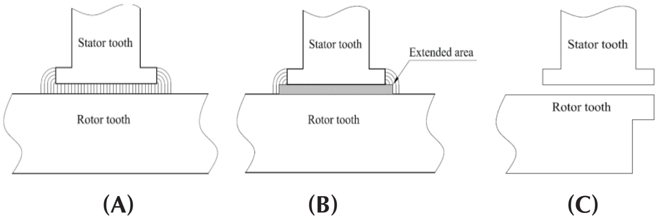

Fig. 6. Replacement of flux fringing paths by extending the overlapped area (A) the flux fringing path under consideration, (B) the overlapped area extension, and (C) the end position for the maximum air-gap permeance area.

One can assume that the starting point for the zero-permeance area (shown in Fig. 7) is the same as the one in the above method. The permeance comparison for this case is shown in Fig. 8. As can be seen from Fig. 8, there is a significant difference between the two air-gap permeances.

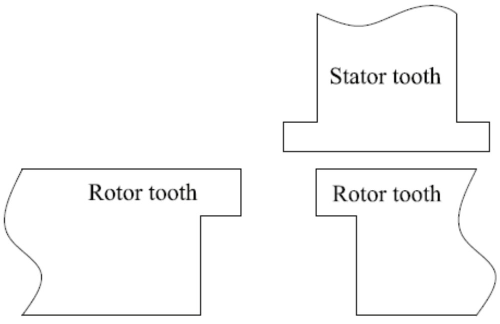

Fig. 7. Position where the air-gap permeance between the stator tooth and the left rotor tooth becomes zero.

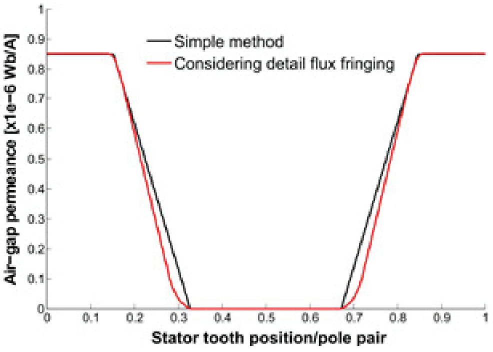

Fig. 8. Air-gap permeance comparison between the two approaches (with the same zero-permeance area).

In order to deal with the error, we suppose a starting point for the zero-permeance area that is earlier than that of the method considering detailed flux fringing paths. In this article, the starting point is assumed to be in the middle of the right edge of the rotor tooth at the point where the permeance considering the fringing path becomes zero. A comparison of the air-gap permeance, accounting for this difference, is displayed in Fig. 9. As seen in Fig. 9, there is a smooth transformation from maximum to zero permeance for the method considering every flux fringing path.

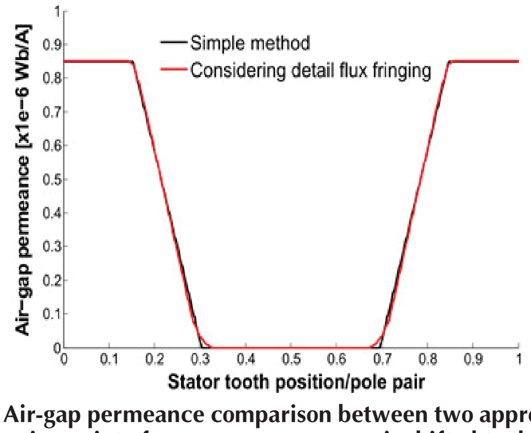

Fig. 9. Air-gap permeance comparison between two approaches (the starting point of zero-permeance area is shifted to the left).

By this simplification, the determination of the air-gap permeance at various rotor angle becomes straightforward. Only five critical positions, corresponding to five different waveforms, need to be determined as seen in Fig. 9. Compared to the 17 positions that must be determined in the previous method, this new method greatly reduces the complexity of the permeance function determination.

Comparison between two methods and with experiments

RN nonlinear equation solving

The system of equations for flux calculations is given by Eq. 7:

$$[P]\times[U]=[\Phi] \tag{7}$$

where *[P]*, *[U]*, and *[ϕ]* are the permeance, magnetic scalar potential, and equivalent flux source matrices, respectively. At each rotor position, the fixed-point method is employed to solve Eq. 7. The new permeability update is expressed by Eq. 8, which was first developed and used by J.C. Wilson (1969) [14]:

$$\mu^{n+1}=\alpha\left(\mu_p^{n+1}-\mu^n\right)+\mu^n \tag{8}$$

where μ^n is the permeability obtained from the n^{th} iteration, μ_p^{n+1} is the provisional permeability computed during the $(n+1)^{th}$ iteration, and α is the relaxation factor. In this paper, α is chosen to be 0.5. The algorithm is explained in Fig. 10. In this algorithm, the maximum number of iterations can be set to avoid infinite loops.

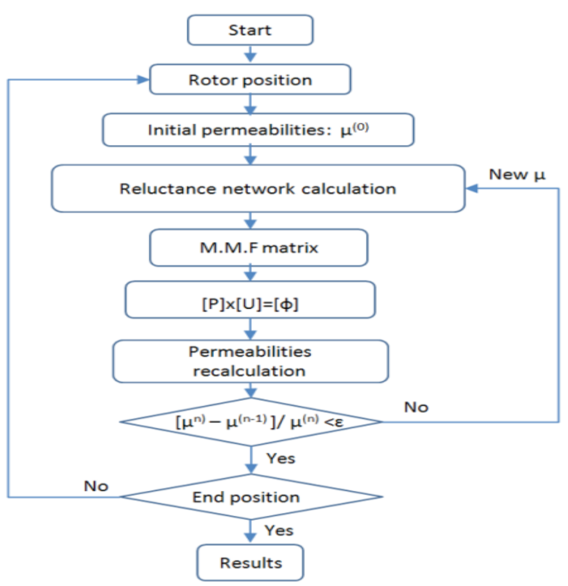

Fig. 10. Algorithm diagram for nonlinear equation solving.

In Fig. 10, the permeability recalculations are based on the B-H curve of the core material. In [15], the permeability is presented as a function of the flux density. This approximation function is advantageous because of the quick computation time and high accuracy due to smooth interpolation when compared to using a look-up table of the original magnetization curve. This permeability fitting function is given by Eq. 9 and is shown in Fig. 11:

$$\mu_B(B)=\mu_0\frac{\frac{1}{K}\sum_{k=1}^{K}\left(\left|\frac{B}{m_k}\right|^{n_k}+a_k^{n_k}\right)^{\frac{1}{n_k}}}{\frac{1}{K}\sum_{k=1}^{K}\left(\left|\frac{B}{m_k}\right|^{n_k}+a_k^{n_k}\right)^{\frac{1}{n_k}}-1} \tag{9}$$

where μ_B is the permeability, which is flux density dependent, K is the approximation order, and a_k, m_k, and n_k are the fitting coefficients. The coefficient b_k is defined such that $a_k=b_k/(b_k-1)$. The values of the coefficients are shown in Table 1. According to Eq. 9, when the flux density increases toward infinity, the permeability approaches the permeability of the air, μ_0.

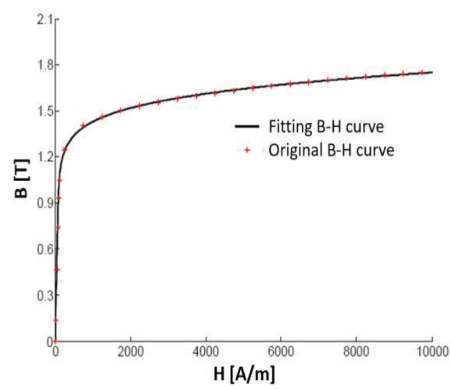

Fig. 11. Magnetization curve of the core material.

Table 1. Fitting coefficients for permeability function.

k	1	2	3	4	5
b_k	1e10	3e6	694	723	111
n_k	6.7	11.8	7.1	12.6	40.0
m_k	19.9	1.9	50.0	21.5	17.6

Result comparisons

The simulations are implemented by MATLAB and done for one pole pair, which is a 60 mechanical degree consisting of 60 points. The computation time is about one second, which is extremely advantageous thanks to the use of the RN method. By the use of the DC excitation windings, the air-gap flux can be easily increased or decreased by controlling the excitation current (I_{dc}). The motor's prototype is displayed in Fig. 12 for the comparison analysis with the RN.

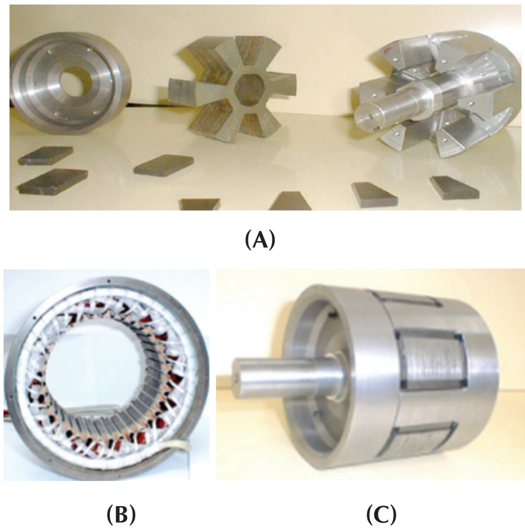

Fig. 12. DESM prototype (A) disassembled rotor, (B) stator, and (C) assembled rotor.

Flux linkage and back EMF: the flux linkage, Ψ, can be computed directly by solving Eq. 7 where the phase back EMFs are found from the derivatives of the phase flux linkage in Eq. 10:

$$e = -\frac{d\psi}{dt} \tag{10}$$

The experimental flux is derived from an integral of the measured winding's voltage. The principle of the DC excitation current supply is shown in Fig. 13 where the excitation winding is represented by the inductance L. With this control circuit, the current excitation direction can be reversed. Fig. 14 compares the flux linkages and back EMFs at a speed of 170 rpm and under a no-load condition. The flux weakening is also tested by injecting a negative DC excitation current of amplitude -3 A. As can be seen from Fig. 14, a good accordance is achieved and there is almost no difference reported in the flux linkage comparisons. However, there is a little difference between the waveforms of the back EMF, which is due to the smoother wave form that leads to a smoother waveform of the back EMF when taking the first derivative. Both methods agree well with the experimental results.

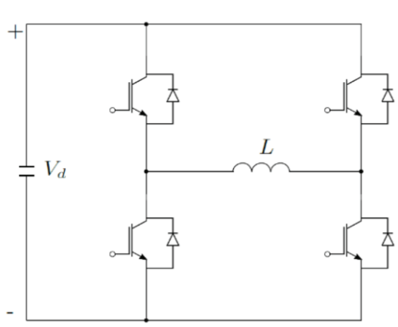

Fig. 13. DC power supply circuit for the excitation windings.

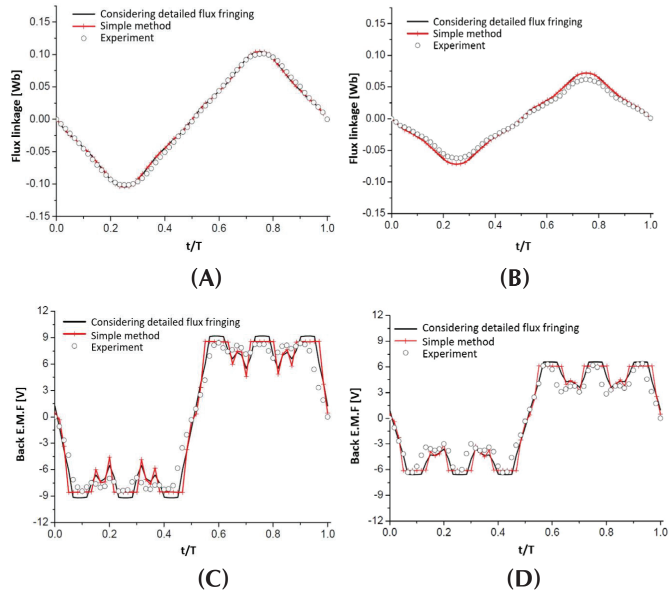

Fig. 14. Comparisons under a no-load condition at 170 rpm (A) flux linkage at I_{dc}=0 A, (B) flux linkage at I_{dc}=-3 A, (C) EMF at I_{dc}=0 A, and (D) EMF at I_{dc}=-3 A.

Electromagnetic torque calculation: in this paper, the electromagnetic torque is calculated by using the virtual work principle, which is based on the derivative of the magnetic co-energy, W_{CO}, with respect to the rotor's angular position, θ, while keeping the phase current constant as in Eq. 11:

$$T_e = \left.\frac{\Delta W_o}{\Delta\theta}\right|_{i=const} \tag{11}$$

The torque comparisons are displayed in Fig. 15 for a range of phase current from zero to the rated value (10 A) and the excitation windings are not excited. The phase shift angle between the EMF and phase current is null. As seen in Fig. 15, a good accordance is reported. In Fig. 16, the torque comparison between the proposed concepts, the RN method considering detailed flux paths, and 3D FEM is presented. In this comparison, an air-gap flux enhancement by a positive excitation current of 3 A is examined. As seen in Fig. 16, the proposed concept agrees well with the two other methods.

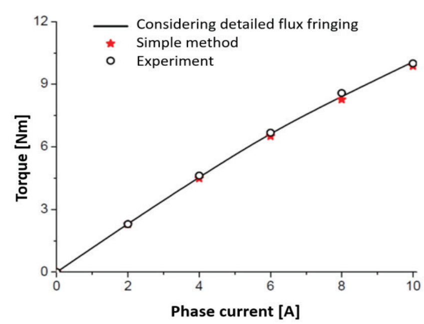

Fig. 15. Torque comparison for various phase currents (I_{dc}=0 A).

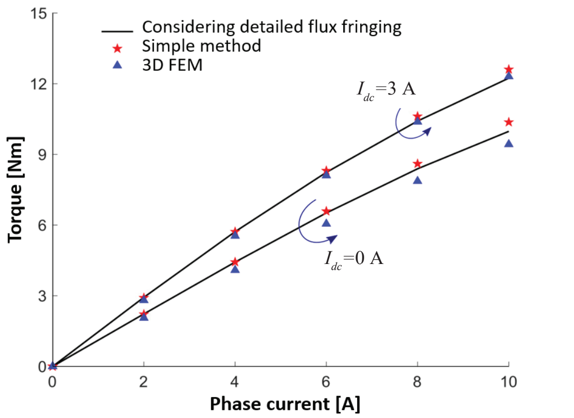

Fig. 16. Torque comparison between RN method and 3D FEM.

Conclusions

This paper has proposed a simple approach for air-gap permeance calculations. The proposed method's convenience and efficiency was shown by comparisons with other methods and measurement. This method is suggested for other machine types with different teeth structures. This method is less time consuming and has a lower complexity in building RN model, which makes the proposed approach quite adaptive to the design phase when a lot of geometry variants must be realised and examined, for example, during the optimisation process.

ACKNOWLEDGEMENTS

This research is funded by Graduate University of Science and Technology under grant number GUST.STS.DT2019-KHVL02. The authors gratefully acknowledge University of Science and Technology of Hanoi for supporting this research.

COMPETING INTERESTS

The authors declare that there is no conflict of interest regarding the publication of this article.

REFERENCES

[1] Y. Amara, L. Vido, M. Gabsi, E. Hoang, A. Hamid Ben Ahmed, M. Lecrivain (2009), "Hybrid excitation synchronous machines: energy-efficient solution for vehicles propulsion", *IEEE Transactions on Vehicular Technology*, **58(5)**, pp.2137-2149.

[2] C. Ilie, M. Mihaiescu, I. Chirita, M. Gutu, M. Popa, N. Tanase (2019), "Synchronous electric generator with double excitation", *11th International Symposium on Advanced Topics in Electrical Engineering (ATEE)*, pp.1-4, DOI: 10.1109/ATEE.2019.8724866.

[3] L. Vido, M. Gabsi, M. Lecrivain, Y. Amara, F. Chabot (2005), "Homopolar and bipolar hybrid excitation synchronous machines", *IEEE International Conference on Electric Machines and Drives*, pp.1212-1218, DOI: 10.1109/IEMDC.2005.195876.

[4] B. Nedjar, S. Hlioui, Y. Amara, L. Vido, M. Gabsi, M. Lecrivain (2011), "A new parallel double excitation synchronous machine", *IEEE Transactions on Magnetics*, **47(9)**, pp.2252-2260.

[5] Y. Hane, K. Nakamura (2018), "Reluctance network model of permanent magnet synchronous motor considering magnetic hysteresis behaviour", *IEEE International Magnetics Conference (INTERMAG)*, Singapore, pp.1-5, DOI: 10.1109/INTMAG.2018.850811.

[6] N. Ullah, F. Khan, W. Ullah, M. Umair; Z. Khattak (2018), "Magnetic equivalent circuit models using global reluctance networks methodology for design of permanent magnet flux switching machine", *15th International Bhurban Conference on Applied Sciences and Technology (IBCAST)*, Islamabad, pp.397-404, DOI: 10.1109/IBCAST.2018.8312255.

[7] K. Nakamura, O. Ichinokura (2008), "Dynamic simulation of Pm motor drive system based on reluctance network analysis", *13th International Power Electronics and Motion Control Conference*, pp.758-762, DOI: 10.1109/EPEPEMC.2008.4635358.

[8] N. Bracikowski, M. Hecquet, P. Brochet, S. Shirinskii (2012), "Multiphysics modeling of a permanent magnet synchronous machine by using lumped models", *IEEE Transactions on Industrial Electronics*, **59(6)**, pp.2426-2437.

[9] J.M. Williams (2004), *Modelling and Analysis of Electric Machines with Asymmetric Rotor Poles Using a Reluctances Based, Magnetic Equivalent Circuit*, Doctoral Dissertation, University of Missouri-Rolla, 202pp.

[10] V. Ostovic (1989), *Dynamics of Saturated Machines*, Springer-Verlag New York, 445pp.

[11] A. Balakrishnan, W. Joines, T. Wilson (1997), "Air-gap reluctance and inductance calculations for magnetic circuits using a Schwarz-Christoffel transformation", *IEEE Transactions on Industrial Electronics*, **12(4)**, pp.654-663.

[12] Z. Zhu, Y. Pang, D. Howe, S. Iwasaki, R. Deodhar, A. Pride (2005), "Analysis of electromagnetic performance of flux-switching permanent-magnet machines by nonlinear adaptive lumped parameter magnetic circuit model", *IEEE Transactions on Magnetics*, **41(11)**, pp.4277-4287.

[13] C. Stuebig, B. Ponick (2008), "Determination of air-gap permeances of hybrid stepping motors for calculation of motor behaviour", *18th International Conference on Electrical Machines,* pp.1-5, DOI: 10.1109/ICELMACH.2008.4800016.

[14] J.C. Wilson (1969), *Theory of the Solid Rotor Induction Machine*, Doctoral Dissertation, University of Colorado, 396pp.

[15] J. Cale, S. Sudhoff, J. Turner (2006), "An improved magnetic characterisation method for highly permeable materials", *IEEE Transactions on Magnetics*, **42(8)**, pp.1974-1981.